RESEARCH ACTIVITIES III
Department of Electronic Structure

III-A Synthesis and Characterization of Exotic Molecule Based Nano-Crystals with Transition Metal Cations : Toward Electron Beam Writing Yielding Metal Dot Arrays and Wires Encapsulated in Carbon Shells

Observation of photoelectron and vibrational spectra of gaseous M–C_2 molecules and clusters, where M = Fe, Co, Ni *etc.*, reminds us high potentiality of these salt-type clusters and nano-crystals for magnetic, catalytic and electronic functionalities. Due to the instability of the carbide compounds, the characterization of the MC_2 compounds has been left unknown. We have found that including MnC_2, all transition metal C_2 salt crystals are ferromagnetic, and that M^{2+}–C_2^{2-} ionic nano-crystals are the best materials for generating nano-metals encapsulated in carbon shells. Annealing or heating above 300 °C induces reduction of cations by anions and resulting segregation of metal atoms by locating C_2 radicals outer and connecting C_2 bi-radicals as graphite-like carbon shells. The relatively low segregation temperatures for FeC_2 and NiC_2 make it possible to draw metallic dots or wire circuits in MC_2 thin layers by scanning electron or laser beams. The small size matrix MC_2 crystals prevent the strong dipole-dipole interaction between the metallic dots, while one can also wash out the matrix salt crystals by acid solution leaving the carbon encapsulated nano-metals on the base plate.

III-A-1 Formation of Air-Stable Fe Nano-Particles in Polar Organic Solution: Fe Nano-Crystals with Graphitic Skin 3.5 nm Thick

KOSUGI, Kentaroh; BUSHIRI, Junaid M. ; NISHI, Nobuyuki

[*Appl. Phys. Lett.* in press]

In the process of investigating formation and characterization of FeC_2 nano-crystals, we found that $Fe^{2+}C_2^{2-}$ salt crystals are ferromagnetic and converted to neutral α-Fe nano-particles encapsulated in graphite-like carbon shells. The thickness of the carbon shells is almost constantly 3.5 nm without regard to size and shape, and corresponds to 10 layers of the graphite sheet, although the shells exhibit curvatures and straight lines bound to the metal core surfaces.

Fine particles of CaC_2 are suspended in acetonitrile solution of $FeCl_2$ and heated in a Pyrex tube situated in a pressure-resistant stainless steel vessel at 250 ºC for 48 hrs. The solution was stirred for the first 4 hrs. but the stirring was stopped the other 20 hrs. The solids obtained on the bottom of the tube contained organic compounds produced by the catalytic reacton of the intermediate product, FeC_2. The black magnetic particles are collected by magnets attached on the side wall of an Erlenmeyer flask and washed by methanol in a ultrasonic cleaning bath three times. Transmission electron microscope (TEM) images of the black deposit are shown in Figure 1. The powder was fixed in an epoxi-resin and sliced to a thickness of approximately 60 nm by a Leica Ultracut UCT microtome. X-ray diffraction pattern of the black deposit was displayed in Figure 2. From the width of α-carbon signals, the average size of the Fe cores is estimated to be 60 nm. At 2θ = 26.0°, a broad signal with asymmetric shape is seen. Bulk graphite shows a sharp peak at 2θ = 26.5°. It is reasonable that we see a peak slightly shifted to lower angle and a wide width correspondent with 3.5 nm thickness. TEM images in Figure 1 clearly show that the thickness of the carbon shells with various shapes and sizes are always 3.5 nm.

In principle, the thermal segregation of FeC_2 should produce Fe and carbon in 1:2 molar ratio. In the TEM observation, we saw amorphous carbon and the metallic Fe particles encapsulated in the carbon shells. The constant thickness of the graphite-like shells suggests the presence of attractive field on the metal core surface. This field must be produced by surface Fe atoms, and thus dependent only on the distance from each surface atom. The size of the particle is not concerned with the field generation. The surface Fe atoms are seen to be in good contact with the shell carbon atoms innermost. This contact may be due to ionic interaction remained only on the surface and the charge separation stabilized by occupation of an excess electron, originally in the carbon shell, in a Rydberg orbital of the cationic Fe atom. This hypothesis can be checked by examining other M(transition metal)C_2 compounds.

In the lower part, a TEM image of Fe-wire encapsulating carbon nano-tube (multi-wall) and an expanded image of its boader area are shown.

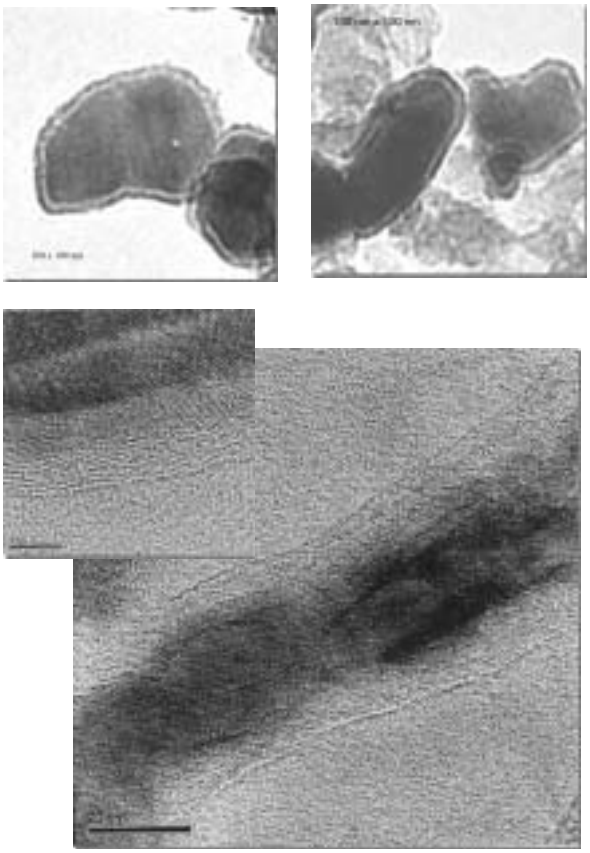

Figure 1. TEM images of α-Fe metallic nano-particles encapsulated in carbon-shell 3.5 nm thick (top) and Fe-wire encapsulating carbon nano-tube(lower).

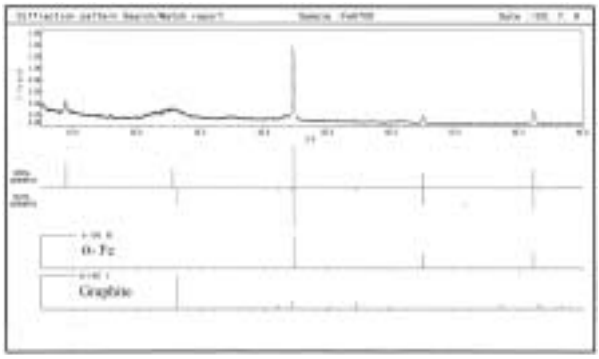

Figure 2. X-ray diffraction pattern of the Fe nano-metals encapsulated in graphite-like carbon shells 3.5 nm thick.

III-A-2 Infrared Absorption Studies of M(transition metal)$^{2+}C_2^{2-}$ Compounds: Bonding Nature and their Stabilities

BUSHIRI, Junaid M. ; KOSUGI, Kentaroh; HINO, Kazuyuki; NISHI, Nobuyuki

Transition metal C_2 compounds have been believed to be non-existent materials. In fact, as far as the metallic part is neutral, the presence of MC_2 is hardly possible due to the inequivalency of the bonding nature of M and C_2. Since C_2 is a di-valent anion, C_2^{2-}, on the other hand, a rock-salt type compound $M^{2+}C_2^{2-}$ can be stabilized by ionic interaction between cations and anions just like CaC_2 and MgC_2. For the synthesis, the simple ion exchange reaction is expected to produce MC_2 salts.

Since CaC_2 reacts with water producing acetylene (C_2H_2) and $Ca(OH)_2$, MCl_2 salt compounds are dissolved in dehydrated acetonitrile. In this solution, fine powders of CaC_2 are suspended and stirred gently. At the temperatures lower than 70 ºC, nothing happens in the solution. At above 75 ºC, the black precipitates are accumulated on the bottom of the reaction vessel.

Figure 1 displays the IR spectra of various ionic MC_2 compounds (M = Ca^{2+}, Mn^{2+}, Fe^{2+}, Co^{2+}, and Ni^{2+}. The doubly degenerated C=C stretching vibration bands of $Ca^{2+}C_2^{2-}$ are seen at 1418 and 1488 cm^{-1}. Among 6 coordinated C_2^{2-} ions, the four C_2^{2-} are located equivalently around the Ca^{2+} ion in a tetrahedral crystal of CaC_2. For one antisymmetric combination of the two C=C stretching oscillators, two sets of symmetric and anti-symmetric oscillators in other two axes split into low energy components and high energy components depending upon in-line (–C=C–Ca–C=C–) configuration or in-parallel configuration of the two C_2 oscillators. Thus the doublet appears around 1450 cm^{-1}. This splitting becomes much narrower in NiC_2.

The Fe–C stretching vibration in the gas phase FeC_2 molecule was found to be 550 cm^{-1} by ZEKE photo-electron spectroscopy (Drechsler *et al., J. Mol. Struct.* **348**, 337 (1995)). In the nano-crystals, a peak of a very broad band is seen at 456 cm^{-1}. The spectral feature of this band is similar to that of MnC_2, while those of CoC_2 and NiC_2 shift to much high frequencies around 600 cm^{-1}. Thus one can see that the M–C bonds in CoC_2 and NiC_2 is strong while those in MnC_2 and FeC_2 are rather weaker. This is in consistent with the reactivity of MC_2 compounds with water. CoC_2 and NiC_2 are stable against water, but MnC_2 and FeC_2 are reactive with water.

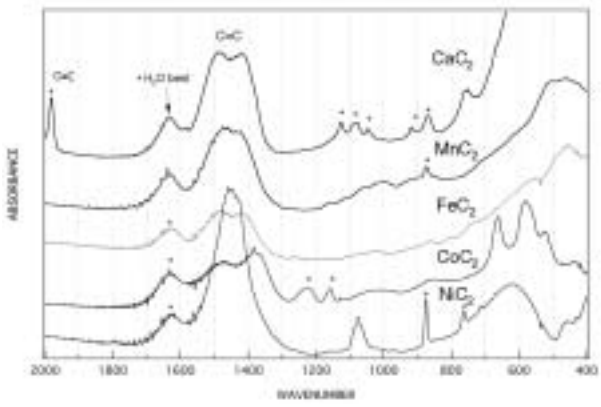

Figure 1. IR Spectra of MC_2 compounds.

III-A-3 Magnetic Behavior of MnC_2 and NiC_2

BUSHIRI, Junaid M.; KOSUGI, Kentaroh; NISHI, Nobuyuki

Most of manganese compounds, such as MnO, MnO_2, MnS, and $MnSO_4$, and pure Mn are antiferro-magnetic. Although pure Ni is ferromagnetic, most of nickel compounds are also antiferromagnetic. Since CoC_2 is ferromagnetic and the spin inversion blocking

temperature increases with increasing size of the nanocrystals, other transition metal acetylide compounds are expected to be ferromagnetic. Magnetic properties of the MnC_2 and NiC_2 nanoparticles synthesized at 78 ºC from their metal chloride compounds and CaC_2 were measured with a SQUID magnetometer (Quantum Design MPMS-7S). The synthesis at this temperature produces mostly several nm size crystals that normally limits the spin inversion blocking temperature lower than the room temperature. MnC_2 particles synthesized at 78 ºC are mostly superparamagnetic but only 10% of the products behaved as magnets at room temperature. MnC_2 particles synthesized at 200 ºC are mostly ferromagnetic exhibit the blocking temperature at 320 K.

Figure 1 displays the temperature change of the magnetic susceptibility of NiC_2 under the zero-field cooling (ZFC) condition and the field cooling (FC) at 50 Oe external field. Although the blocking temperature is seen at 10 K, the hysteresis curve at 1.85 K exhibits the cohesive force as large as 1,660 Oe. Annealing of this sample at 300 ºC for 2 hours changes the average size of 10–20 nm and the blocking temperature increases higher than room temperature.

NiC_2 particles are stable at the atmospheric condition, while MnC_2 is damaged by water in the atmosphere. On heating above 250 ºC, NiC_2 shows segregation into metallic nickel and carbon.

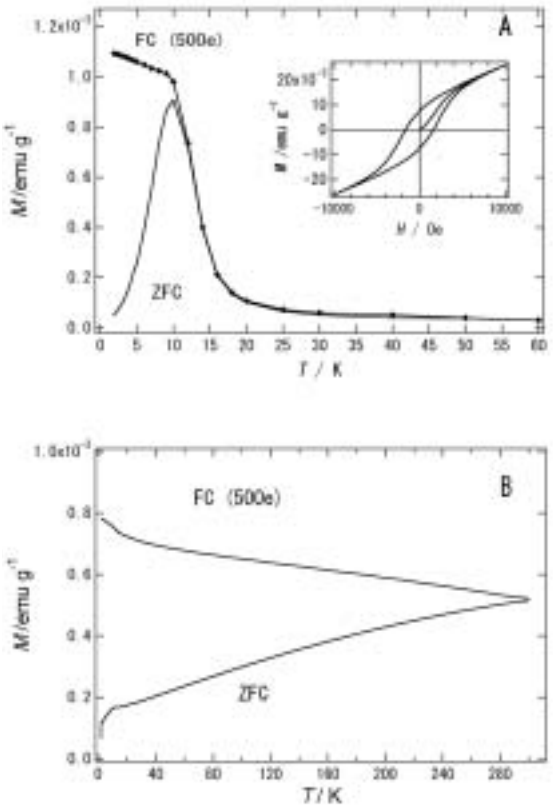

Figure 1. Temperature changes of magnetic susceptibility(*M*) of NiC_2 nanocrystals synthesized at 75 °C (**A**) and measured under the zero-field cooling condition (ZFC) and the field cooling (FC) condition. Inserted in **A** is a magnetic hysteresis curves at 1.8 K. Annealing at 300 °C for 2 hours produced 10 nm-size particles and the *M-T* curves change drastically as seen in B.

III-A-4 XAFS and XANES Studies of CoC_2

KOSUGI, Kentaroh; BUSHIRI, Junaid M.; HINO, Kazuyuki; YOKOYAMA, Toshihiko; NISHI, Nobuyuki

$Co^{2+}C_2^{2-}$ nano-clusters are ferromagnetic in contrast with antiferromagnetic electronic structure of $Co^{2+}O^{2-}$. CoC_2 nanoparticles are synthesized from acetonitrile solution of $CoCl_2$ with suspended CaC_2 fine powder. The products obtained from the solution at 340 K is called Sample LT (low temperature product). The CoC_2 nanoparticles are also synthesized from the thermal or photochemical reaction of $Co_4(CO)_{12}$ with solvent CH_2Cl_2. The particles are embedded in amorphous carbon. This sample is called Sample ME (matrix embedded).

XANES: The peak at 7724 eV seen for Sample LT coincides with that of hydrated Co^{2+} ion (as seen for $Co(NO_3)_2(6H_2O)$ suggesting that the Co is in a divalent cation state. The matrix embedded sample (Sample ME) also exhibits the peak at the same energy, while the width is expanded. This is in accord with the appearance of C_2^{2-} infrared absorption bands.

XAFS: The Fourier transform spectrum of XAFS signals of Sample ME exhibited a little difference from that of Sample LT, particularly in the region from 3.2 ~ 4.5 Å. As clearly seen from the appearance of water bands in IR spectra, the two samples contain coordinated water molecules. Therefore the peaks at 1.6 Å (2.08 Å after phase factor correction) are contributed from both Co–C and Co–O pairs. It is very difficult to analyze this peak. The peak at 2.80 Å (3.18 Å after phase factor correction) and other main peaks at much longer distances are attributed to Co–Co pairs. There is little contribution from the direct Co–Co bond at 2.05 Å (2.5 Å after phase factor correction). We have found, however, that the presence of oxygen gas in the solvent results in the appearance of the 2.05 Å peak. The de-oxygenation treatment in a globe box by Ar bubbling longer than 6 hours is necessary . On the basis of the assumption that the Co–C pairs hardly contribute to the peaks at distances longer than 3.5 Å, the Fourier transform spectra of Sample ME are analyzed with the models presented in Figure 1. Most of peaks are reproduced nicely, while the discrepancies in intensities between the calculated and observed spectra become serious at longer distances. This is thought due to the structural disorder in nano-particles. The observed spectra shows drastic intensity decrease at longer distances.

The structure of Sample ME is close to that of MgC_2. The structures derived from the analyses for Sample LT and Sample ME are shown on the top and the bottom of Figure 1.

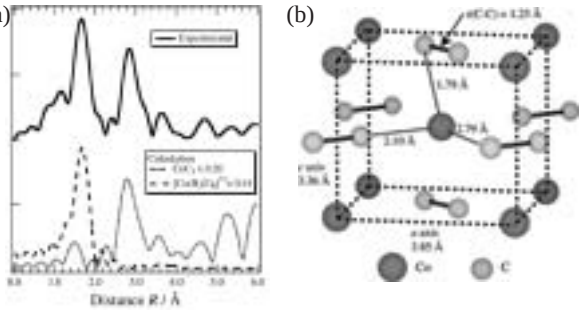

Figure 1. (a) Fourier transform of EXAFS signal. (b) Structure model of CoC_2.

III-A-5 Matrix Embedded Cobalt-Carbon Nano-Cluster Magnets: Behavior as Room Temperature Single Domain Magnets

NISHI, Nobuyuki ;KOSUGI, Kentaroh; HINO, Kazuyuki; YOKOYAMA, Toshihiko

[*Eur. J. Phys. D* **24**, 97 (2003)]

A new type of Co–C nanoparticles is synthesized from CH_2Cl_2 solution of $Co_4(CO)_{12}$ by heating up to 210 ºC in a closed vessel. Transmission electron microscope (TEM) as shown in Figure 1 and electron energy loss spectroscopy (EELS) observation show that the particles are embedded in amorphous carbon and their average size is 12 nm. The radial structure function obtained from the extended X-ray absorption fine structure (EXAFS) of the Co *K*-edge absorption of the Co–C nanoparticles provides a Co–C average distance of 2.08 Å, and the Co–Co distances of 3.18 Å , and 3.9 (±0.2) Å . The particles exhibit the magnetic hysteresis curve with a coercive force of 200 Oe at 20 K and 260 Oe at 300 K. The temperature dependence of the magnetic susceptibility measured under zero-field cooling and 10 Oe field cooling conditions exhibits the behavior characteristic of a set of single magnetic domain nanomagnets in an amorphous carbon matrix.

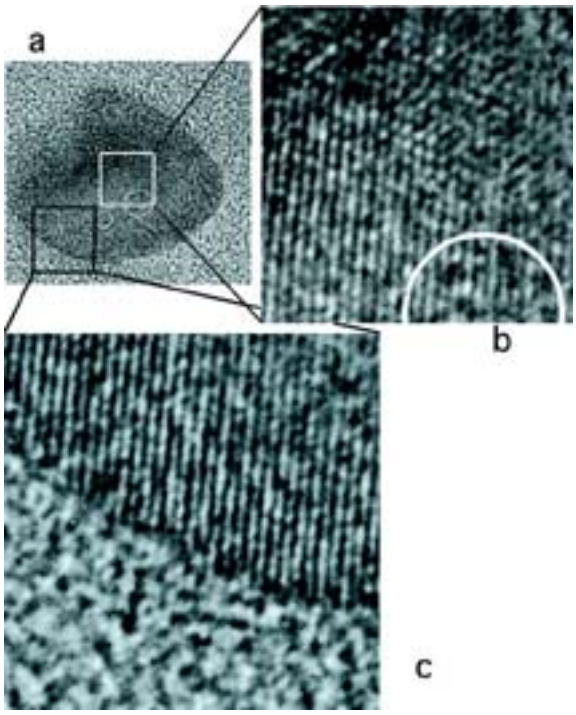

Figure 1. TEM image of a CoC_2 nano-crystal (a). Expanded images (b and c) show tetragonal lattice structure of the crystal.

III-B States of Neutral and Ionic Molecular Associates in Solutions

States of molecular associates particularly in aqueous solutions are of great importance in understanding the role of molecules in living organisms. We found that any ideally mixed state cannot be seen in protic-protic mixtures such as water-alcohol, water-acetic acid, and alcohol-acetic acid systems on the molecular level at solute molar fractions (χ_A) higher than 0.001. In such a system, solute-solute asociation is highly favored resulting in microscopic phase separation. In this year, we studied the aqueous mixture of *N*,*N*-dimethylacetamide (DMA), and have shown that hydrogen bonding between the C=O group and the water molecules and structural changes of predominant solvent clusters were taking place at these specific mole fractions of DMA in aqueous solution.

III-B-1 Structure of Aqueous Mixture of N,N-Dimethylacetamide Studied by Infrared Spectroscopy, X-Ray Diffraction, and Mass Spectrometry

TAKAMUKU, Toshiyuki; MATSUO, Daisuke; TABATA, Masaaki; YAMAGUCHI, Toshio; NISHI, Nobuyuki

[*J. Phys. Chem. B* **107**, 6070 (2003)]

Infrared (IR) spectroscopy and X-ray diffraction measurements have been performed at 298 K on mixtures of *N*,*N*-dimethylacetamide (DMA) and water over the entire range of DMA mole fractions (χ_{DMA}). Mass spectra have also been measured on the clusters that have been isolated by the adiabatic expansion of liquid droplets of the mixtures. The IR overtone band of the C=O stretching vibration for the DMA–D_2O mixtures and the O–D stretching band of HDO for the DMA–H_2O mixtures containing 5% D_2O both shifted to lower frequencies as the water content increased,

accompanied by two inflection points, at χ_{DMA} = 0.1 and 0.6. These results suggested that hydrogen bonding between the C=O group and the water molecules and structural changes of predominant solvent clusters were taking place at these specific mole fractions. The X-ray radial distribution functions have indicated that the structure of the predominant solvent clusters in the mixtures could be classified into four regimes: (1) $0 < \chi_{DMA} \leq 0.1$, where the water clusters predominate; (2) $0.1 < \chi_{DMA} \leq 0.3$, where more water clusters than DMA clusters are formed; (3) $0.3 < \chi_{DMA} \leq 0.6$, where the DMA structure becomes predominant but the water clusters still remain; and (4) $0.6 \leq \chi_{DMA} \leq 1$,where the DMA clusters are dominant in the mixtures. On the basis of the present results on the microscopic structure of the mixtures, the anomalies of thermodynamic parameters such as the enthalpy of mixing are discussed.

III-C Ultrafast Dynamics and Scanning Tunneling Microscopy

For the study of molecules on metallic or crystalline surface, very low temperature Scanning Tunneling Microscope (LT STM) system are now in use for collaboration with users in universities. Ultrafast laser systems with pico and femtosecond time resolutions are also available.

III-C-1 Low Temperature Scanning Tunneling Microscopy for Sub-Nanoscale Systems

WATANABE, Kazuo[3]; OHSHIMO, Keijiro[1]; INOKUCHI, Yoshiya; NAKABAYASHI, Takakazu[2]; NAGATA, Takashi[3]; NISHI, Nobuyuki
([1]RIKEN; [2]Hokkaido Univ.; [3]Univ. Tokyo)

Scanning tunneling microscopy/spectroscopy (STM/STS) is one of the most powerful tools for the real-space observation and the identification of sub-nanoscale materials on the surface. By combining with the ultrashort light pulses, it provides ultimate resolutions of both time and space. Figure 1 shows our STM apparatus which consists of two liquid helium cooled STM heads operating in the ultra-high-vacuum ($\sim 2 \times 10^{-11}$ Torr). The two heads are connected to a sample preparation chamber equipped with an argon ion sputter gun, a gas dosing system, a pulse injection system for the deposition of nanoparticles and bio-molecules, a quadrupole mass spectrometer, and a LEED/AES optics. The STM head (A) is cooled down to 10 K. It has a pair of UV compatible viewing ports from which the sample can be irradiated at ~ 20 K *in situ*. The output pulses (λ = 189 ~ 11200 nm, 4 ps) are introduced through the window from two independently tunable picosecond OPA systems with an optical delay stage. The STM head (B) is cooled below 4 K and used for STS studies. Figure 2 shows an STM image of an Au_{12} cluster (provided by Tsukuda's group) on a graphite surface at 10 K. The size of the cluster is measured ~ 0.8 Å, which is close to the TEM (Transmission Electron Microscope) results. STS investigation of the electronic structures of the nanoclusters is underway. We have also observed the adsorption structure of nitrous oxide molecules on a Pd(110) surface at 10 K (a joint project with Prof. Matsushima's Lab of Hokkaido University).

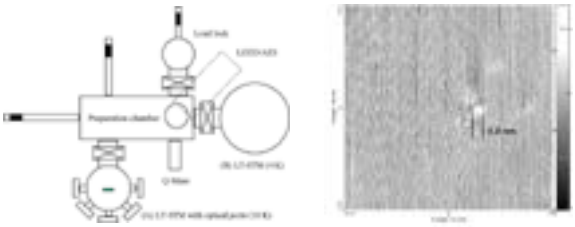

Figure 1. Schematic drawing of the experimental setup.

III-C-2 Ultrafast Time-Resolved Study of *N*-Salicilideneaniline in the Isolated State

OKABE, Chie[1]; NAKABAYASHI, Takakazu[2]; INOKUCHI, Yoshiya; SEKIYA, Hiroshi[1]; NISHI, Nobuyuki
([1]Kyushu Univ.; [2]Hokkaidou Univ.)

N-salicylideneaniline (SA) is a well-known photochromic aromatic anil. The photoexcitation of the $^1(\pi,\pi^*)$ state of the enol form produces the keto form *via* the excited state intramolecular proton transfer (ESIPT). To investigate ultrafast processes in the photoexcited SA, we have applied the femtosecond time-resolved resonance-enhanced multiphoton ionization technique under the isolated conditions. Figure 1 shows the decay profiles of the photoexcited SA measured by the excitation of the enol form with pump wavelength at 320 nm and probe wavelengths at 395 and 790 nm. The time profile in Figure 1 (a) is fitted with three decay components < 230 fs, 1.5 ps, and > 100 ps, while the time profile in Figure 1 (b) is reproduced by the convolution of < 230 fs and 3.5 ps decay components. The < 230 fs decay component is attributed to ultrafast ESIPT from the $^1(\pi,\pi^*)$ state of enol form to the cis-keto form. The 3.5 ps and 1.5 ps decay components are assigned to the ion signal from the $^1(n\pi^*)$ state of the enol form and that the $^1(\pi\pi^*)$ state of the *cis*-keto form produced *via* ESIPT, respectively. We have first to observe the $^1(n\pi^*)$ state of the enol form. The excitation wavelength dependence of ESIPT has been examined in the region from 360 to 373 nm. The rise time of the keto form is less than several hundreds fs even for the

excitation near the red-edge of the absorption of the enol form. In addition, the rise time of the keto form shows no significant OH/OD isotope effect. These results indicate that the ESIPT reaction occurs within several hundreds fs, and the barrier height to ESIPT from the $^1(\pi,\pi^*)$ state is low.

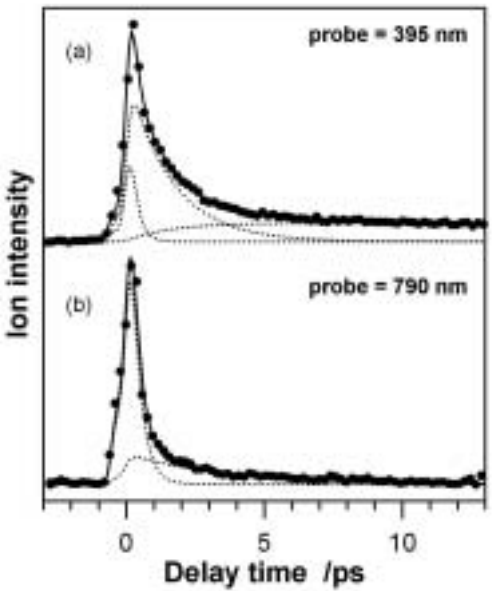

Figure 1. Time evolutions of ion signal of SA detected by femtosecond REMPI with pump wavelength at 320 nm and two different probe wavelengths at 395 nm.

III-C-3 Picosecond Time-Resolved Stokes and Anti-Stokes Raman Studies on the Photochromic Reactions of Diarylethene Derivatives

OKABE, Chie[1]; NAKABAYASHI, Takakazu[2]; FUKAMINATO, Tuyoshi[1]; KAWAI, Tsuyoshi[1]; IRIE, Masahiro[1]; SEKIYA, Hiroshi[1]; NISHI, Nobuyuki
([1]Kyushu Univ.; [2]Hokkaidou Univ.)

[*J. Phys. Chem. A* **107**, 5384 (2003)]

The cyclization and cycloreversion reactions of diarylethene derivatives have been studied with picosecond time-resolved Stokes and anti-Stokes Raman spectroscopies. The cyclization reaction of 1,2-bis(2,5-dimethyl-3-thienyl)perfluorocyclopentene (DMTF) is found to occur within 4 ps to produce the vibrationally excited closed forms in the ground electronic (S_0) state. The time constant of the vibrational relaxation toward a thermal equilibrium with solvent molecules is estimated to be about 10 ps. The cycloreversion reaction of 1,2-bis(3,4-dimethyl-5-phenyl-2-thienyl)perfluorocyclopentene (DMPTF) also generates the vibrationally excited open forms in the S_0 state within 4 ps, which decay on a picosecond time scale. The picosecond time-resolved anti-Stokes Raman spectra of DMPTF show two vibrational bands assignable to the C=C stretching modes of the cyclopentene and thiophene moieties of the generated open forms. The Raman intensity arising from the cyclopentene moiety relative to that from the thiophene moiety becomes smaller with the delay time, indicating that part of the excess energy generated *via* the cycloreversion reaction is localized on the C=C stretching mode of the cyclopentene moiety. This result suggests that the C=C stretching mode of the cyclopentene moiety is one of the promoting or the accepting modes in the cycloreversion reaction.

III-D Spectroscopic and Dynamical Studies of Molecular Cluster Ions

Electron defficiency of molecular cluster cations can attract electron rich groups or atoms exhibiting charge transfer or charge resonance interaction in the clusters. This causes dynamical structural change such as proton transfer or ion-core switching in hot cluster ions or clusters in solution.

III-D-1 Positive Charge Distribution in $(Benzene)_1(toluene)_2^+$ and $(Benzene)_2(toluene)_1^+$ Studied by Photodissociation Spectroscopy

INOKUCHI, Yoshiya; OHASHI, Kazuhiko[1]; SEKIYA, Hiroshi[1]; NISHI, Nobuyuki
([1]Kyushu Univ.)

[*J. Chem. Phys.* **117**, 10648 (2002)]

The positive charge distribution in benzene–toluene hetero-trimer ions is investigated by photodissociation spectroscopy in the near-infrared (6000–14000 cm^{-1}) and infrared (2800–3150 cm^{-1}) regions. The electronic spectra of $(benzene)_1(toluene)_2^+$ and $(benzene)_2(toluene)_1^+$ in the near-infrared region display the strong bands at 9430 and 8330 cm^{-1}, respectively. These bands are ascribed to the charge resonance band; the positive charge is not localized on a single molecule. The vibrational spectrum of $(benzene)_1(toluene\text{-}d_8)_2^+$ shows three distinct bands at 3054, 3084, and 3108 cm^{-1}; these bands are assigned to the CH stretching vibrations of the benzene moiety. The similarity of the spectral features to those of the neutral benzene monomer suggests that the benzene molecule in the $(benzene)_1(toluene)_2^+$ ion has a neutral character. The positive charge is localized on the toluene dimer unit with a structure written as

$(toluene)_2^+\cdots(benzene)_1$. The vibrational spectrum of $(benzene)_2(toluene)_1^+$ bears a resemblance to that of $(benzene)_2^+$. The vibrational spectrum of $(benzene\text{-}d_6)_2(toluene)_1^+$ shows dissimilar features to the spectrum of the neutral toluene monomer, suggesting that a certain amount of the positive charge is carried by the toluene moiety. These results are explained by the charge resonance interaction between $(benzene)_2$ and $(toluene)_1$. A simple perturbation theory is applied for determining the positive charge distribution in $(benzene)_2(toluene)_1^+$. The probability of finding the charge on the $(benzene)_2$ and $(toluene)_1$ moieties is analyzed to be 58 and 42%, respectively.

III-D-2 Infrared Photodissociation Spectroscopy of [Aniline–$(Water)_n$]$^+$ (n = 1–8)

INOKUCHI, Yoshiya; HONKAWA, Yoshiki[1]; OHASHI, Kazuhiko[1]; SEKIYA, Hiroshi[1]; NISHI, Nobuyuki
([1]Kyushu Univ.)

[*J. Phys. Chem. A* **107**, 4230 (2003)]

Infrared photodissociation spectra of [aniline–$(H_2O)_n$]$^+$ (n = 1–8) are measured in the 2700–3800 cm^{-1} region. The spectra are interpreted with the aid of density functional theory calculations. A substantially red-shifted and broadened transition is distinctly observed at 3105 cm^{-1} for the n = 1 ion, and assigned to the stretching vibration of the hydrogen-bonded NH oscillator of the aniline$^+$ moiety. The spectrum of the n = 2 ion demonstrates a large perturbation to both of the NH oscillators, indicating that each NH bond is bound to a water molecule in the most stable structure. For the n = 3 ion, three broad bands exist at 3070, 3230, and 3420 cm^{-1}, and there are two maxima and a weak hump at 3637, 3723, and 3696 cm^{-1}. The calculated spectrum of the 2-1 branch structure resembles the observed one very well. For the n = 4 ion, there exist three strong bands at 2960, 3100, and 3430 cm^{-1}, and a very weak one at 3550 cm^{-1}. The observed spectrum in the 3600–3800 cm^{-1} region is decomposed into four bands at 3640, 3698, 3710, and 3734 cm^{-1}. These bands are originated from the 2-2 branch isomer except for the 3550 and 3710 cm^{-1}bands. These two bands are due to the other isomer that has the five-membered ring. A characteristic transition in the observed spectrum of the n = 5 ion is the 3684 cm^{-1}band, which hardly emerges in the spectra of n = 1–4. This band is assigned to the free OH stretching vibration of the three-coordinated (double-acceptor–single-donor) H_2O, indicating the ring structure. The n = 5 ion has the five-membered ring structure with the fifth water molecule bound to the terminal (double-acceptor) H_2O. The observed spectra of the n = 6–8 ions show features quite different from those of n = 1–5; a very strong and broad band emerges around 3400 cm^{-1}. It is suggested that the n = 6–8 ions have the proton transfer form with some ring structure.

III-D-3 Infrared Spectra and Structures of $(CH_3NH_2)_nH^+$ (n = 1–4). Binding Features of an Excess Proton

MICHI, Takayuki[1]; OHASHI, Kazuhiko[1]; INOKUCHI, Yoshiya; NISHI, Nobuyuki; SEKIYA, Hiroshi[1]
([1]Kyushu Univ.)

[*Chem. Phys. Lett.* **371**, 111 (2003)]

Infrared photodissociation spectra of $CH_3NH_3^+$–**Ar** and $(CH_3NH_2)_nH^+$ with n = 2–4 are measured in the 2600–3500 cm^{-1} region and analyzed with the aid of ab initio calculations. The intensities of the CH-stretching transitions relative to the NH-stretching transitions increase with increasing n, suggesting the change of the binding features of an excess proton in the clusters. Two CH_3NH_2 molecules in $(CH_3NH_2)_2H^+$ equally share the proton. On the other hand, the proton is localized on the central molecule in $(CH_3NH_2)_4H^+$, forming the CH_3-NH_3^+ core solvated by three CH_3NH_2 molecules.

III-D-4 Fermi Resonance Interaction in Hetero-Dimer and Trimer Ions Containing Aniline$^+$

INOKUCHI, Yoshiya; OHSHIMO, Keijiro; OHASHI, Kazuhiko[1]; HONKAWA, Yoshiki[1]; SEKIYA, Hiroshi[1]; NISHI, Nobuyuki
([1]Kyushu Univ.)

[*Chem. Phys. Lett.* **373**, 568 (2003)]

Vibrational spectra of hetero-dimer and trimer ions containing aniline$^+$ are measured by infrared photodissociation spectroscopy. For the dimer ions, the NH_2 bending overtone band gains its intensity through Fermi resonance interaction with the hydrogen-bonded NH stretching fundamental. Unperturbed frequencies of the NH_2 bending overtone are calculated to be in the range of 3255–3276 cm^{-1}, suggesting that the frequency is almost intact upon cluster formation. For the trimer ions, Fermi resonance interaction occurs mainly between the NH_2 bending overtone and the stretching fundamental of the NH oscillator involved in the stronger hydrogen bond.

III-D-5 Infrared Spectra and Structures of Aniline$^+$–Furan and Aniline$^+$–Phenol: Preference between *p*-Type and *s*-Type Hydrogen-Bonded Structures

HONKAWA, Yoshiki[1]; INOKUCHI, Yoshiya; OHASHI, Kazuhiko[1]; NISHI, Nobuyuki; SEKIYA, Hiroshi[1]
([1]Kyushu Univ.)

[*Chem. Phys. Lett.* **376**, 244 (2003)]

Infrared photodissociation spectra of aniline$^+$–M (M = thiophene, furan and phenol) are measured in the 2700–3700 cm^{-1} region and analyzed by density functional theory calculations. Only a structure with a π-type hydrogen bond is found for aniline$^+$–thiophene. Two structural isomers are identified for aniline$^+$–furan and aniline$^+$–phenol, which have either a π-type or a σ-type hydrogen bond, where an amino proton of aniline$^+$ interacts with the π-electrons or the oxygen atom of the

neutral molecules, respectively. The isomer with a σ-type hydrogen bond is more stable for aniline$^+$–phenol, while less stable for aniline$^+$–furan.

III-D-6 Infrared Photodissociation Spectroscopy of Protonated Formic Acid and Acetic Acid Clusters

INOKUCHI, Yoshiya; NISHI, Nobuyuki

[*J. Phys. Chem. A* in press]

Infrared photodissociation spectra of protonated formic acid clusters, $H^+\cdot(HCOOH)_{2-5}$, are measured in the 3000–3700 cm^{-1} region. Density functional theory calculation is applied to $H^+\cdot(HCOOH)_{2-5}$. Geometry optimization of $H^+\cdot(HCOOH)_{2-5}$ indicates that stable forms of these clusters are open chain structures with free OH groups at both ends. In the infrared photodissociation spectra of the n = 2 and 3 species, there are two sharp bands in the range of 3400–3700 cm^{-1}. The lower- and higher-frequency bands of them are attributed to the free OH stretching vibrations of the peripheral COOH groups in the *E* and *Z* conformations, respectively. The intensity of the higher-frequency band relative to that of the lower-frequency one decreases from n = 2 to 3. The n = 4 and 5 ions show only one sharp band in the same region. This band is assigned to the free OH stretching vibrations of the end COOH groups in the *E* conformation; the n = 4 and 5 ions have the peripheral COOH groups only in the *E* conformation. We observe infrared photodissociation spectra of $H^+\cdot(HCOOH)_{6,7}$ in the 3500–3600 cm^{-1} region. The absence of any free OH band for n = 7 shows that both ends of chain structures of n = 7 are terminated by cyclic dimers. Infrared photodissociation spectra of $H^+\cdot(CH_3COOH)_{2-5}$ are also examined in the 3000–3700 cm^{-1} region. Resemblance of the spectra of $H^+\cdot(CH_3COOH)_n$ to those of $H^+\cdot(HCOOH)_n$ suggests that the acetic acid clusters have structures similar to those of the formic acid clusters; the intermolecular network is formed only by the COOH groups.